



Mathematical modeling and interpretation of equilibrium isotherms of Pb (II) from aqueous media by *Chlorella pyrenoidosa* immobilized in *Luffa cylindrica*

Imane Nouacer¹ · Mokhtar Benalia¹ · Ghania Henini² · Mebrouk Djedid¹ · Ykhlef Laidani²

Received: 9 April 2021 / Revised: 21 June 2021 / Accepted: 29 June 2021 / Published online: 31 July 2021
© The Author(s), under exclusive licence to Springer-Verlag GmbH Germany, part of Springer Nature 2021

Abstract

New sorbent was prepared from unicellular green microalgal *Chlorella pyrenoidosa* (CP) immobilized in *Luffa cylindrica* (CP-LC) as a biosorbent for the removal of lead ions from aqueous media in a batch experiment mode. The prepared biosorbent was characterized by Fourier transform infrared spectroscopy (FTIR) and scanning electron microscopy (SEM). In the experimental design of the Pb (II) removal process, the equilibrium isotherms were studied and modeled. To select the best-fit isotherm model for this biological process, the experimental data were fitted in the eighteen different types of one-, two-, three-, four-, and five-parameter isotherm models. A comparison of non-linear models for selecting the optimum isotherm showed Fritz–Schlunder (V) model gives the most accurate fit to describe the experimental data, determined based on several error functions. Taking into account the outcome and in an attempt to optimize the equilibrium isotherms, the equation of Fritz–Schlunder (V) was modified to obtain more sophisticated model and more precision parameters values. As a consequence of such a developed model to existing mentioned ones, the mathematical model developed in this study is more suitable for predicting the equilibrium data. According to the results obtained, the evaluation of experimental data in terms of biosorption kinetics elucidated that the biosorption of Pb (II) by CP-LC well followed pseudo-second-order kinetics. The maximum biosorbent capacity of CP-LC was found to be 123 mg/g for 40 min at pH5. The calculated thermodynamic factors (ΔG° , ΔH° , and ΔS°) indicated that the biosorption process was favorable, spontaneous, and exothermic at 298–318 K.

Keywords *Chlorella pyrenoidosa* · *Luffa cylindrica* · Isotherms · Kinetics · Mathematical model · Pb (II) removal

Nomenclature

A_k (mg/g)	Koble-Carrigan isotherm constant	b_{KH} (L/g)	Constant in Khan isotherm
ae (-)	Activity of Pb (II) in solution at equilibrium	b_R (-)	Constant in Redlich–Peterson isotherm
a_{kh} (-)	Constant in Khan isotherm	B_T (Kj/mol)	Temkin constant
a_R (L/g)	Constant in Redlich–Peterson isotherm	b_T (Kj/mol)	Adsorption energy
ARE	average relative error	C (L/g)	Fritz-Schlunder (IV) constant
A_T (L/g)	Equilibrium binding constant	C_0 (mg/L)	Initial Pb (II) ion concentration
as	Activity of adsorbed Pb (II)	Ce (mg/L)	Pb (II) ion concentration in solution at equilibrium
b_o (L/g)	Constant in Baudu isotherm	Cs (mg/g)	Pb (II) adsorbed on CP-LC
B_k (L/g)	Koble-Carrigan isotherm constant	CP	<i>Chlorella pyrenoidosa</i>
		CP-LC	<i>Chlorella pyrenoidosa</i> immobilized in <i>luffa cylindrica</i>
		D (L/g)	Fritz-Schlunder (IV) constant
		ERSQ (-)	Sum of the squares of the errors
		GM	Growth medium
		HYBRID	Hybrid fractional error function
		IUPAC	International union of pure and applied chemistry
		K (-)	Henry's isotherm model adsorption constant

✉ Imane Nouacer
i.nouacer@lagh-univ.dz

¹ Department Process Engineering, Faculty of Technology, University Amar Telidji-Laghouat, B.P 37G, 03000 Laghouat, Algeria

² Department Process Engineering, Faculty of Technology, University Hassiba Ben Bouali Chlef, P.O Box.151, 02000 Chlef, Algeria

K_1 (1/min)	The rate constant of pseudo first-order model	R (J/mol K)	Ideal gas constant
K_2 (g/mg/min)	the rate constant of pseudo second-order model	R^2 (-)	Coefficient of determination
K_c (-)	The distribution constant	R_L (-)	Separation factor
K_{KI} (L/g)	Kiselev equilibrium constant	S^2	Residual variance
K_{K2} (-)	Constant of complex formation between adsorbed molecules	SEM	Scanning electron microscopy
K_E (L/mg)	Elovich constant	t (min)	Time
K_F (mg/g) ^{1/n}	Adsorption capacity	T (K)	Temperature
K_{FH} (L/g)	Flory–Huggins equilibrium constant	W (KJ/mol)	Interaction energy between adsorbed molecules
K_{FG} (L/g)	Fowler–Guggenheim equilibrium constant	x, y (-)	Constants in Baudu isotherm
K_{FS1} (L/g)	Fritz-Schlünder (v) equilibrium constant	Y_e (-)	Activity coefficient of Pb (II) in equilibrium solution
k_{FS2} (L/g)	Fritz-Schlünder (v) equilibrium constant	Y_s (-)	Activity coefficient of adsorbed Pb (II)
K_H (L/g)	Hill–de Boer constant	ΔH° (kJ/mol)	Enthalpy change
K_L (L/mg)	Constant in Langmuir isotherm	ΔS° (J/mol)	Entropy change
K_n (kJ/mol)	Energetic constant of the interaction between adsorbed molecules	K	
K_R (L/g)	Constant in Redlich–Peterson isotherm	ΔG° (kJ/mol)	Gibbs free energy change
K_{RP} (L/g)	Constant in Radke–Prausnitz isotherm		
k_s (L/g)	Constant in Sips isotherm	Greek symbols	
K_T (L/g)	Constant in Toth isotherm	\emptyset (-)	Surface coverage of the adsorbent
m (g/L)	Dose of free or immobilized cells	α, β (-)	Constant in modified Fritz-Schlunder (v)
M_1, M_2 (-)	Constants in Fritz-Schlünder model		
MPSD	Marquardt's percent standard deviation		
N (-)	Number of observations in the experimental isotherm		
n (-)	Constant in Freundlich isotherm		
n_{FH} (-)	Number of adsorbates occupying adsorption sites		
n_K (-)	Noefficient in Koble-Carrigan isotherm		
n_R (-)	Constant in Radke–Prausnitz isotherm		
n_S (-)	Coefficient in Sips isotherm		
n_T (-)	Constant in Toth isotherm		
P (-)	Number of parameters in the regression model		
q_{cal} (mg/g)	Estimate from the isotherm for corresponding q_{exp}		
q_e (mg/g)	Adsorption capacity		
q_{exp} (mg/g)	Observation from the batch experiment		
q_{mKH} (mg/g)	Maximum adsorbate uptake from Khan model		
q_m (mg/g)	Maximum adsorbate uptake from Radke–Prausnitz model		
q_{mb} (mg/g)	Maximum adsorbate uptake from Baudu model		
q_{max} (mg/g)	Maximum adsorbate uptake from Langmuir model		
q_{mE} (mg/g)	Maximum adsorbate uptake from elovich model		
q_{mFS} (mg/g)	Fritz-Schlünder (v) maximum adsorption capacity.		
q_{mk} (mg/g)	Maximum adsorbate uptake from Toth model		
q_{mS} (mg/g)	Maximum adsorbate uptake from sips model		

1 Introduction

With the rapid development of various neo-industrial activities (including vehicle emissions, textile, leather, mining, tannery, galvanizing, electroplating, pigment and dyes, metallurgical and paint industrial discharges, and heavy metal-containing fertilizers), wastes containing different toxic metallic substances are discharged directly or indirectly into the natural environment increasingly, especially in economically developing countries, having brought a massive increase in pollution and threatened human health [1, 2]. Furthermore, metallic substance as a kind of resource is becoming rarer and rarer. The toxic properties of heavy metal ions are presented as follows: (1) the degree of toxicity can last for a long time in the environment; (2) some heavy metals could be transformed from a low toxic element into high toxic forms in a certain environment; (3) the bioaccumulation and bioaugmentation of these metals by the food chain in living species could damage normal physiological activity and endangering human life; (4) heavy metals can only be changed and transformed in valence and species, but cannot be degraded by any methods; (5) the toxicity of heavy metal ions occurs even in very low concentration of about 1.0–10 mg/L [2]. Among the metal ions that are hazardous to the environmental system, lead ions that have mutagenic properties and highly toxic are a major pollutant that must be eliminated due to their threat to the ecosystem and human health; researches showed that lead

ions can attack the nervous system and brain, cause behavioral disorders and intellectual disabilities, and damage several organ systems including the liver and kidneys. The symptoms of this metal poisoning include insomnia, vertigo, anemia, headaches, hallucinations, weakness, and mortality [1, 3]. Considering lead toxicity and its abundance, it is important to accurately detect its existence and concentration to mitigate its adverse effects. As such, the advancement and of development effective and accurate lead ion sensors are important and will have numberless applications [3]. Due to these reasons, a wide variety of conventional processes have been studied in detail to achieve the aim of metal removal from contaminated aqueous media. Some of the treatment methods used to overcome this environmental problem are ion exchange, reverse osmosis, membrane separation method, flocculation, chemical precipitation, electro-coagulation, ultra-filtration, etc. [4]. Unfortunately, most of these conventional methods cannot be used on a wide scale because of their significant downsides such as incomplete removal, low selectivity, prohibitively expensive, high energy consumption, or generation of large quantities of toxic wastes. An alternative treatment process to sequester heavy metals is biosorption, which utilizes various inexpensive biomass of biological origin [2], owing to the large variety of biomaterials available and their capacity to promote metals retention. Among the biological supports that have the ability to bond with heavy metal ions, it is possible to point out the microorganisms, algae, and lignocellulosic materials. These biomaterials can be originated in the ecosystem and produced for commercialization application or designated as residue from agricultural and fermentative processes [5]. The main elements found in these biomaterials are cellulose and hemi-cellulose, and also organic and inorganic elements in smaller percentages. As a result of their composition, microalgae have several functional groups that can efficiently bind with certain pollutants present in the aqueous media such as heavy metals ions and thus are considered excellent biological supports for the removal of metals ions through the biosorption process [5, 6]. The biosorption mechanism information is the most important part of the information in interpreting a biosorption process. An equilibrium model of relationships known as adsorption isotherms describes how solute sorbate reacts with the sorbent materials; thus, an accurate mathematical model description of the equilibrium adsorption isotherms is important to the effective expression of the affinity of sorbent and potential of adsorbents and effective design of the sorption mechanism [7]. In this present study, an attempt was to explore the feasibility of an efficient biosorbent obtained by coating microalgal species (*Chlorella pyrenoidosa*) on the surface of lignocellulosic material (*Luffa cylindrica* discs) for the removal of lead ions from aqueous solution; in this regard, the various parameters that control the biosorption were optimized, followed by a thermodynamic and kinetic study. More specifically, the

experimental data were analyzed in this paper using eighteen isotherm models obtained by a nonlinear regression method. Another purpose of this study was to explore the applicability of the several error function in determining the best fitting isotherm models. Finally, the most important part of this work is the adjustment of the Fritz-Schlünder (V) model and its application to the data of Pb (II) onto free and immobilized *C. pyrenoidosa* in *Luffa cylindrica*.

2 Materials and methods

2.1 Preparation of the biosorbent

2.1.1 Organism and culture medium

The unicellular green microalgae, *C. pyrenoidosa*, was maintained by subculturing on 1/5% YMG agar slants (yeast extract 4 g, malt extract 10 g, and D-glucose 6 g per liter of distilled water). The growth medium (GM) consisted of (grams per liter of distilled water) KNO₃, 2; KH₂PO₄, 0.1; MgSO₄·7H₂O, 0.1; CaCl₂·H₂O, 0.05; H₃BO₃, 0.00286; MnCl₂·4H₂O, 0.00181, ZnSO₄·7H₂O, 0.00022; NaMoO₄·2H₂O, 0.0004; CuSO₄·5H₂O, 0.00008; FeSO₄·7H₂O, 0.00557; and Na₂ EDTA, 0.00745. The pH was adjusted to 7.5 and the temperature was fixed at 303 K under illumination (16:8 day-night cycle) at 20 μmol photons m⁻² s⁻¹ in 1-L Erlenmeyer flask. The microalgae were harvested by centrifugation at 5000 rpm for 15 min and washed with distilled water and then used for sequester of Pb (II) from an aqueous solution.

2.1.2 Preparation of *C. Pyrenoidosa*–*Luffa cylindrica* immobilized discs

A weighted portion of 1 g of *Luffa cylindrica* discs was transferred to 100 mL of GM medium and inoculated with 5 mL, 30-day-old stationary phase cultures of *C. pyrenoidosa* and incubated for 14 days for developing inoculum biomass. The luffa discs were removed and washed thoroughly with fresh GM to remove any free microalgae cells. The *C. pyrenoidosa*–luffa sponge immobilized discs were harvested after 3 weeks, washed thoroughly with distilled water, and freeze-dried for further studies on metals biosorption.

2.2 Determination of heavy metal concentration

A stock solution of lead ions (1000 mg/L) was prepared by solubilizing a determined amount of Pb (NO₃)₂ in deionized water. Diluted concentrations were obtained from the stock solution. The pH of solutions was adjusted by adding diluted solutions to 0.1M HCl or NaOH. The residual concentration of lead ions left in an aqueous solution was determined using

an AAS-UNICAM-969 atomic absorption spectrophotometer.

2.3 Batch sorption studies

The biosorption equilibrium isotherms of lead ions were studied in the batch method. All experiments were carried out with 1 g biosorbent and 100 mL of the analyzed metals having the initial concentrations of 10–300 mg/L solution in a 250-mL flask at 298 K and with a stirring speed of 150 rpm for 40 min. Each experiment was performed in triplicate. In the tests, the amount of metal ions biosorbed per gram of immobilized and free cells of *C. pyrenoidosa* for Pb (II) ions were determined separately. The solid was separated and the supernatants were digested using nitric acid-perchloric acid. The removal efficiency of Pb (II) is calculated by the following formula [8]:

$$R\% = \frac{C_0 - C_e \times 100}{C_0} \quad (1)$$

where C_0 and C_e are the initial and final concentrations of metal ions in the solution (mg/L). The amount of adsorbed Pb (II) per unit mass of adsorbent at time t (q_t mg/g) was obtained by using the following formula [9]:

$$q_e = \frac{(C_0 - C_e)}{m} \quad (2)$$

where C_e is the equilibrium concentrations of the metal ions (mg/L) in solution, and m is the dose of free or immobilized cells (g/L).

To obtain information on the main functional groups present on the surface of the biosorbent particles and to determine the active sites in free and immobilized *C. pyrenoidosa*, Fourier transform infrared spectroscopy (FTIR) was used. A mass of 0.1 g of biosorbent was ground and encapsulated in 1 g of KBr, and FTIR spectra were obtained with an IR Prestige-21, Shimadzu spectrometer. The FTIR data were obtained at wavenumbers of 400–4000 cm^{-1} . The morphology of biomass was characterized by scanning electron microscopy (SEM) (HIT S2600 N).

3 Theory

3.1 Biosorption kinetics

Biosorption kinetic expresses the mechanism of biosorption. The solute sorbate can be transferred from the liquid phase to the surface of the biosorbent in several steps, and the combination of one or more steps can be speed control mechanisms. The transfer of adsorbate can be either in the form of mass transfer of the solution surrounding the outside of the adsorbent via the outer boundary layer film, or diffusion of the

sorbate molecules into a biosorption zone through solution absorption pores, or by a biosorbent surface diffusion mechanism, or chemical or physical (internal or external) [1]. In biosorption of lead (II), pseudo-first-order and pseudo-second-order kinetic models were applied to investigate the potential speed control steps. Non-linear form equations of kinetic models applied for biosorption.

Kinetics of Pb (II) are given as:

$$q_t = q_e(1 - e^{-k_1 t}) \quad (3)$$

$$q_t = \frac{K_2 q_e^2}{1 + K_2 q_e t} \quad (4)$$

where q_t and q_e are the biosorption capacity (mg/g) at equilibrium and at time t (min), respectively, and k_1 (1/min) is the rate constant of pseudo-first-order model K_2 (g/mg/min) is the rate constant of pseudo-second-order model [1].

3.2 Equilibrium sorption models

One of the fundamental criteria for adsorbent materials utility is its maximal sorption capacity, which is obtained based on the relationship between the mass of sorbate per mass unit of sorbent (mg/g) and the equilibrium concentration of sorbate (mg/L). The best design of the adsorption process requires a mathematical model description of an isotherm under equilibrium conditions. In this regard, several mathematical models of one-, two-, three-, four-, and five-parameter available for interpreting the experimental data. The parameters of each isotherm can provide insights into the circulation of solute sorption between the sorbent/sorbate phases, the adsorption mechanism, and the affinity of the adsorbent [10]. The linear and nonlinear mathematical equations of isotherm models are given in Table 1. In the present study, eighteen different isotherm equations were studied for analyzing the experimental data. These models are Henry, Langmuir, Freundlich, Temkin, Elovich, Fowler-Guggenheim, Kiselev, Hill de Boer, Flory-Huggins, Redlich-Peterson, Sips, Koble-Carrigan, Radke-Prausnitz, Toth, Khan, Baudu, Fritz-Schlünder (IV), and Fritz-Schlünder (V).

3.3 Error functions

The goodness-of-fit measures were determined based on the error functions. The best-fit isotherm model was identified based on the lowest error distribution between the predicted and experimental values. The model with the minimum value of error functions is considered to be the most suitable isotherm model. In this regard, several mathematical error functions such as the coefficient of determination (R^2), residual variance (S^2), the average relative error (ARE), the sum of the squares of the errors (ERSQ), the hybrid fractional error

Table 1 Illustration of the linear forms, nonlinear forms, and plot of various isotherm models analyzed for optimization studies [11, 12]

	Non-linear form	Linear form	Plot	N° eq
One parameter model Henry	$q_e = KC_e$ a	-	q_e Vs C_e	(5)
Two parameter models Freundlich	$q_e = K_F C_e^{(1/n_F)}$ b	$\log q_e = \log K_F + \frac{1}{n_F} \log C_e$	$\log q_e$ Vs $\log C_e$	(6)
Langmuir	$q_e = q_{max} K_L \frac{C_e}{1 + K_L C_e}$ c R_L $= \frac{q_{max}}{(1 + K_L C_e)} \frac{C_e}{C_0}$ d	$\frac{C_e}{q_e} = \frac{1}{K_L} + \frac{C_e}{q_{max}}$	$\frac{C_e}{q_e}$ Vs C_e	(7)
Elovich	$C_e = \frac{q_e}{q_{mE}} K_E \exp\left(\frac{-q_e}{q_m}\right)$ e	$\ln \frac{q_e}{C_e} = \ln K_E - \frac{q_e}{q_m}$	$\ln \frac{q_e}{C_e}$ Vs q_e	(8)
Temkin	$q_e = \frac{RT}{b_T} \ln A_T C_e$ f	$q_e = \frac{RT}{b_T} \ln A_T + \frac{RT}{b_T} \ln C_e$	q_e vs $\ln C_e$	(9)
Fowler–Guggenheim	$K_{FG} C_e = \left(\frac{\emptyset}{1-\emptyset}\right) \exp\left(\frac{2W_A}{RT}\right) \mathbf{g}$	$\ln C_e \left(\frac{1-\emptyset}{\emptyset}\right) = \ln K_{FG} + \left(\frac{2W_A}{RT}\right)$	$\ln C_e \left(\frac{1-\emptyset}{\emptyset}\right)$ Vs \emptyset	(10)
Kiselev	$K_{K1} C_e = \left(\frac{\emptyset}{1-\emptyset}\right) (1 + K_{K2} \emptyset)$ h	$\frac{1}{C_e(1-\emptyset)} = \left(\frac{K_1}{1-\emptyset}\right) + (K_2 K_1)$	$\frac{1}{C_e(1-\emptyset)}$ Vs $\left(\frac{\emptyset}{1-\emptyset}\right)$	(11)
Hill–de Boer	$K_H C_e = \left(\frac{\emptyset}{1-\emptyset}\right) \exp\left(\frac{\emptyset}{1-\emptyset} - K_n \frac{\emptyset}{RT}\right)$ i	$\ln \left(\frac{C_e(1-\emptyset)}{\emptyset}\right) - \left(\frac{\emptyset}{1-\emptyset}\right) = -\ln K_1 + K_n \left(\frac{\emptyset}{RT}\right)$	$\ln \left(\frac{C_e(1-\emptyset)}{\emptyset}\right) - \left(\frac{\emptyset}{1-\emptyset}\right)$ VS \emptyset	(12)
Flory–Huggins	$\frac{\emptyset}{C_0} = K_{FH} (1-\emptyset)^{n_{FH}}$ J	$\ln \left(\frac{\emptyset}{C_0}\right) = \ln K_{FH} + n_{FH} (1-\emptyset)$	$\ln \left(\frac{\emptyset}{C_0}\right)$ Vs $(1-\emptyset)$	(13)
Three parameter models Redlich–Peterson	$q_e = K_R \frac{C_e}{1 + a_R C_e} b_R$ k	$\ln(K_R C_e q_e - 1) = b_R \ln C_e + \ln a_R$	$\ln \left(\frac{C_e}{q_e}\right)$ Vs $\ln C_e$	(14)
Sips	$q_e = q_{ms} \frac{K_S C_e^{n_S}}{1 + K_S C_e^{n_S}}$ l	$\ln \left(\frac{q_e}{q_m - q_e}\right) = \frac{1}{n_S} \ln C_e + \ln K_S$	$\ln \left(\frac{q_e}{q_m - q_e}\right)$ Vs $\ln C_e$	(15)
Koble–Carrigan	$q_e = \frac{A_K C_e^{n_K}}{1 + B_K C_e^{n_K}}$ m	$\frac{1}{q_e} = \frac{1}{A_K C_e^{n_K}} + \frac{B_K}{A_K}$	$\frac{1}{q_e}$ vs $\frac{1}{C_e^{n_K}}$	(16)
Radke–Prausnitz	$\emptyset = K_T \frac{C_e}{(1 + K_T C_e)^{n_T}}$ n	$\ln \left(\frac{q_e}{q_m - q_e}\right) = n_T \ln K_T + n_T \ln C_e$	$\ln \left(\frac{q_e}{q_m - q_e}\right)$ Vs $\ln C_e$	(17)
Toth	$q_e = q_{mK} \frac{b_{KH} C_e}{1 + b_{KH} C_e}$ p	-	-	(18)
Khan	$q_e = q_{mb} \frac{C_e^{1+x}}{1 + b_0 C_e^{1+x}}$ q	-	-	(19)
Four and five parameter models				
Baudu				
Fritz–Schlunder (IV)	$q_e = \frac{C C^{M1}}{1 + D C^{M2}}$ r	-	-	(21)
Fritz–Schlunder (V)	$q_e = q_{mFS} \frac{K_{FS1} C^{M1}}{1 + K_{FS2} C^{M2}}$ s	-	-	(22)

K: Henry’s isotherm model adsorption constant
K_F: (mg/g)(L/mg)^{1/n} adsorption capacity, (1/n) :adsorption intensity
q_e and **q_{max}**(mg/g): equilibrium and the maximum adsorbate uptake, **K_L** (L/mg): the Langmuir isotherm constant, **C_e** (mg/L): the concentration of adsorbate at equilibrium
R_L: the separation (dimensionless) factor
K_E (L/mg): Elovich equilibrium constant, **q_{mE}** (mg/g) maximum adsorbate uptake from Elovich model
A_T (L/g): equilibrium binding constant. **b_T** (Kj/mol): adsorption energy. **R** (J/mol · K) ideal gas constant. **T** (K) temperature
K_{FG} (L/g): Fowler–Guggenheim equilibrium constant, **W** (KJ/mol): interaction energy between adsorbed molecules. **∅**: surface coverage of the adsorbent
K_{K1} (L/g): Kiselev equilibrium constant. **K_{K2}**: constant of complex formation between adsorbed molecules
K_H (L/g): Hill–de Boer constant. **K_n** (kJ/mol): energetic constant of the interaction between adsorbed molecules
K_{FH} (L/g): Flory–Huggins equilibrium constant. **n_{FH}**: number of adsorbates occupying adsorption sites
a_R (L/g): constant in Redlich–Peterson isotherm, **K_R** (L/g): constant in Redlich–Peterson isotherm. **b_R** constant in Redlich–Peterson isotherm.
q_{ms} (mg/g): maximum adsorbate uptake from sips model. **ks** (L/g): constant in Sips isotherm. **n_S**: coefficient in Sips isotherm
A_K (mg/g): Koble-Carrigan isotherm constant. **B_K**(L/g): Koble-Carrigan isotherm constant, **n_K**: coefficient in Koble-Carrigan isotherm
q_m (mg/g): maximum adsorbate uptake from Radke–Prausnitz model. **K_{RP}** (L/g): constant in Radke–Prausnitz isotherm **n_R** coefficient in Radke–Prausnitz isotherm
q_{mK} (mg/g): maximum adsorbate uptake from Toth model. **K_T** (L/g): constant in Toth isotherm. **n_T**: coefficient in Toth isotherm
q_{mKH} (mg/g): maximum adsorbate uptake from Khan model. **b_{KH}** (L/g): constant in Khan isotherm. **a_{kh}**: constant in Khan isotherm
q_{mb} (mg/g): maximum adsorbate uptake from Baudu model. **b₀** (L/g): constant in Baudu isotherm ,x and y are constant in Baudu isotherm
C (L/g): Fritz-Schlunder (IV) constant. **D** (L/g): Fritz-Schlunder (IV) constant. **M₁** and **M₂** are constant in Fritz-Schlunder model
q_{mFS} (mg/g) Fritz-Schlunder (v) maximum adsorption capacity. **K_{FS1}** and **K_{FS2}** (L/g) are Fritz-Schlunder (v) equilibrium constant

function (HYBRID), and Marquardt’s percent standard deviation (MPSD) were examined in this work to make a comparison between experimental results and the predicted model, to

select the most suitable fit isotherm to experimental data. The minimum value of error function assessments will indicate the similarity of isotherm to the experimental data. The

mathematical expression of the error equations is illustrated in Table 2, where n is the number of data points, p is the number of parameters in the model, and q_{exp} and q_{cal} are respectively the experimental and calculated values of sorption capacity of metal ions in the solid phase (mg/g) [11]:

3.4 Desorption and regeneration studies

To carry out the regeneration and desorption studies of immobilized *C. pyrenoidosa* biomass, five different desorption agents, tap H₂O, distilled water, 0.1 M HCl, 0.1 M H₂SO₄, and 0.1 M NaOH, were utilized to desorb the lead (II) from the biosorbent. Exactly, 100 mL of the desorption agents was kept in 250-mL Erlenmeyer flasks with the recovered biosorbent and agitated for 30 min with continuous agitation at a 100 rpm at a temperature of 298 K. The regenerated biosorbent was used in five consecutive adsorption/desorption cycles to determine the reusability of the immobilized *C. pyrenoidosa* onto *Luffa cylindrica*. The final metal ion concentrations in the aqueous solution were determined. The desorption and reloading ratio was calculated mathematically as follows[13]:

Desorption ratio

$$= \frac{\text{Amount of metal ions desorbed}}{\text{Amount of metal ions adsorbed}} * 100 \quad (5)$$

Reloading ratio

$$= \frac{\text{Amount of metal loaded in a higher cycle}}{\text{Amount of metal loaded in the first cycle}} * 100 \quad (6)$$

4 Results and discussion

4.1 Biosorbent characterization

To further investigate the biosorption process, the free and immobilized *Chlorella pyrenoidosa* was observed under

scanning electron microscopy (Fig. 1). As shown in Fig. 1a, the image of *C. pyrenoidosa* showed a uniform spherical morphology, and it is possible to remark the presence of pores with an average diameter of 1.80 μm, classified as macropores confirming by the International Union of Pure and Applied Chemistry (IUPAC). Thus, the selectivity of the adsorption process should be more related to the interactions with the surface function groups and not with the pore size [5]. The SEM micrograph of *C. pyrenoidosa* immobilized in *Luffa cylindrica* thread showed a uniform microalgal growth along the surface of the LC fiber thread confirming that immobilized *C. pyrenoidosa* cells were not fixed at a single point. This uniform distribution in CP-LC is an important criterion for the removal of metallic substances. Representative SEMs of single *Luffa cylindrica* before and after immobilization are depicted in Fig. 1b, c.

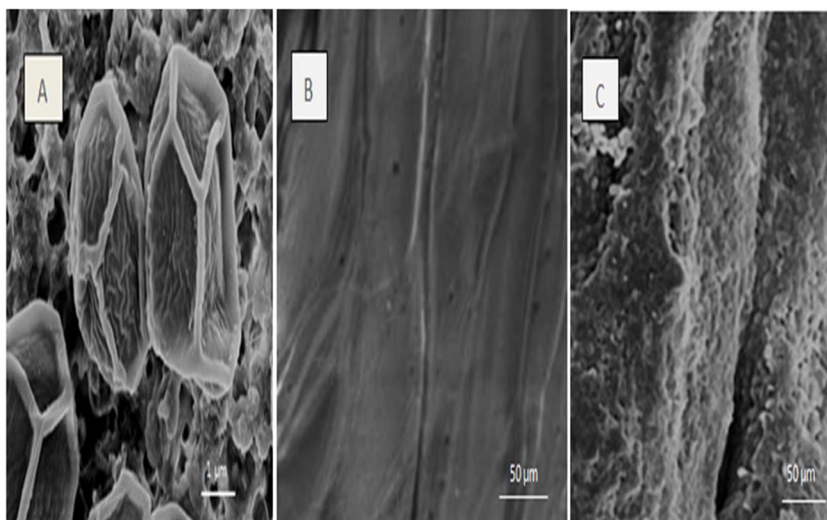
The pattern of sorption of metal ions onto biomaterials is attributable to the functional groups present on active sites and characteristic bonds present on them. Figure 1 depicts the FTIR spectrum determined for *Luffa cylindrica* (LC), *Chlorella pyrenoidosa* (CP), and *C. pyrenoidosa* immobilized in *Luffa cylindrica* (CP-LC). A broadband from 3600 to 3100 cm⁻¹ may be observed in the *Luffa cylindrica* spectrum, which is indicative of the elongation of –OH groups [10]. The bands located at 2810–2850 cm⁻¹ correspond with the oscillation band of the group –CH [14, 15]. The intense peak near the 1500 cm⁻¹ region is typical of *Luffa cylindrica* and indicative of C=O vibrations. The weak band at 1450 cm⁻¹ is ascribed to COO⁻ associations and indicates the presence of carboxyl groups in the *Luffa cylindrica* molecules. The peak that appeared at 950 cm⁻¹ is attributed to the oscillation of C–O, while the oscillation band at 930 cm⁻¹ is assigned COC groups [10].

A wideband ranging between 3600 and 3000 cm⁻¹ is the fingerprint of the oscillation of OH groups in the spectra of *C. pyrenoidosa* and confirms the existence of a hydroxide group [16]. The absorption peak at 2800 cm⁻¹ could be attributed to the presence of asymmetric and symmetric –CH groups [10]. Another peak at 1500 cm⁻¹ suggesting the oscillation of C=O (extension of amide I) indicates the presence of residual N-acetyl groups

Table 2 Error functions used in the study [11].

Error function	Equation	N° eq
The coefficient of determination (R ²)	$\frac{(q_{exp} - q_{cal})^2}{\sum (q_{exp} - q_{cal})^2} + \frac{(q_{cal} - q_{cal})^2}{\sum (q_{cal} - q_{cal})^2}$	(23)
Residual variance (S ²)	$\frac{\sum (q_{exp} - q_{cal})^2}{n - p}$	(24)
The average relative error (ARE)	$\frac{100}{n} \sum_{i=1}^n \left \frac{q_{exp} - q_{cal}}{q_{cal}} \right $	(25)
The sum of the squares of the errors (ERSQ)	$\sum_{i=1}^n (q_{exp} - q_{cal})^2$	(26)
The hybrid fractional error function (HYBRID)	$\frac{100}{n - p} \sum_{i=1}^n \left(\frac{(q_{cal} - q_{exp})^2}{q_{cal}^2} \right)^{\frac{1}{n}}$	(27)
Marquardt's percent standard deviation (MPSD)	$100 \sqrt{\frac{1}{n - p} \sum_{i=1}^n \left(\frac{q_{cal} - q_{exp}}{q_{cal}} \right)^2}$	(28)

Fig. 1 **a** SEM of *C. pyrenoidosa* cells. **b** SEM of *Luffa cylindrica* fiber. **c** SEM of *C. pyrenoidosa* immobilized in *Luffa cylindrica*

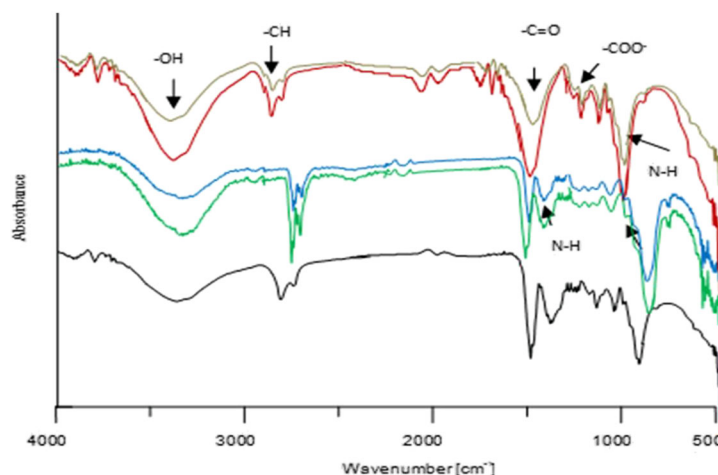


[17]. The intense bands at 1470 cm^{-1} and 1100 cm^{-1} relate to oscillations of the N–H with exists as amine groups in *Chlorella pyrenoidosa* [10]. One of the fundamental monosaccharides in *Chlorella pyrenoidosa* is glucosamine, an amino sugar, and thence, the presence of the amide groups might represent this amino sugar [18]. Distinct bands at 960 cm^{-1} (extension of C–O group) and at 930 cm^{-1} (extension of COC- bond) confirms the a-L-guluronic acid of *C. pyrenoidosa* [19]. In turn, the spectra of *C. pyrenoidosa* immobilized in *Luffa cylindrica* adsorption peaks typical of both compounds constituting the sorbent applied in the study. A new peak, which does not exist in pure *C. pyrenoidosa*, is an asymmetric peak of adsorption at 1350 cm^{-1} being typical of the COO^- bands. It indicates that the CP-LC occurs carboxyl groups origin native *Luffa cylindrica*. The CP-LC spectrum depicts also a shift of the absorption peak from 1500 to 1450 cm^{-1} and disappearance of the amine group band (1500 cm^{-1}), which elucidates the reaction proceeding between *L. cylindrica* and *C. pyrenoidosa* as a consequence of ionic interactions between the positively charged amine group of *C. pyrenoidosa* and negatively charged carbonyl group of *L. cylindrica*. To control the functional groups involved in the biosorption of Pb (II) onto CP and CP-LC, a comparison between the FTIR spectrum before and after biosorption of Pb (II) was done (Fig. 2). FTIR spectra depict slight changes in functional groups and surface characteristics of the biosorbents, elucidated by the shift of some functional groups' peaks due to lead biosorption. Furthermore, the fact demonstrated that the lead ions were successfully adsorbed by the CP and CP-LC was probably via physical interactions between the lead ions and the functional groups present. These shifts could be attributed to the changes in lead (II) ions associated with

carboxylate and hydroxylate anions, indicating that acidic groups, carboxyl, and hydroxyl are a predominant contributor to the complexation of lead ions and ion exchange processes [20].

4.2 Effect of pH

It is well documented that solution's pH is an important factor that has a significant influence on the metal solubility and the sorbate concentration of the counter ions on the functional group of the biosorbent. Thus, pH is considered the most important factor that could affect the biosorption of metal ions from aqueous solutions [9]. Figure 3 depicts the effect of pH variation on the biosorption of Pb (II) ions onto free and immobilized *C. pyrenoidosa*. The efficiency of Pb (II) biosorption in a pH in a range from 4.5 to 6 reached 91.36% for CP and 97% for CP-LC. Consequently, all the experiments were adjusted out at pH 5. The current outcome indicated that the biosorption of Pb (II) was increased with an increment in pH value. Thus, at lower pH, Pb (II) would be present commonly as M (II) ions. The minimum biosorption showed at low pH of 2 could be, on the one hand, due to the fact that the presence of higher proton concentration and its mobility favored hydronium ions biosorption parallel to M (II) ions and, on the other hand, owing to the great solvability and ionizability of metal salt in the acidic solution. It would be credible to suggest that at a lower pH value, the adsorbent surface is surrounded by H_3O^+ ions, thereby preventing the positively charged metal ions from approaching the binding sites of the biomass surface. This condition suggests that the surface of biomass becomes more positively charged such that the attraction between active sites and metal cations is decreased. In contrast, when the pH level increased, the binding efficiency incremented because the functional groups of



FTIR spectra of: — L C, — CP, — Pb (II)–CP, — CP-LC, — Pb (II)–CP-LC.

Fig. 2 FTIR spectra of: — L C, — CP, — Pb (II)–CP, — CP-LC, — Pb (II)–CP-LC.

biomass surface were negatively charged thus facilitating biosorption of M (II); it could be deduced that the biosorption yield of Pb (II) increased with increasing pH as the metal species become less stable in the solution [21]. The optimum biosorption observed in the pH range from 4.5 to 6 could be due to partial hydrolysis of metal cations, which favors **electrostatic attraction** between the surface of biosorbents and Pb^{2+} ions. Resulting in the formation of soluble hydroxylated complexes of $M(OH)^+$ ions and $M(OH)_2$, which would be adsorbed to a considerable extent on a less-polar carbon surface of the biomass as regards M (II) ions [22]. The Pb (II) ions are presumably adsorbed at the surface of biomass by ion-exchange mechanism or via hydrogen bonding as previously mentioned as follows [22]:

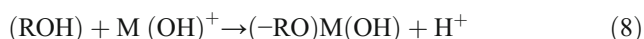
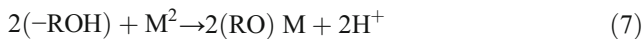
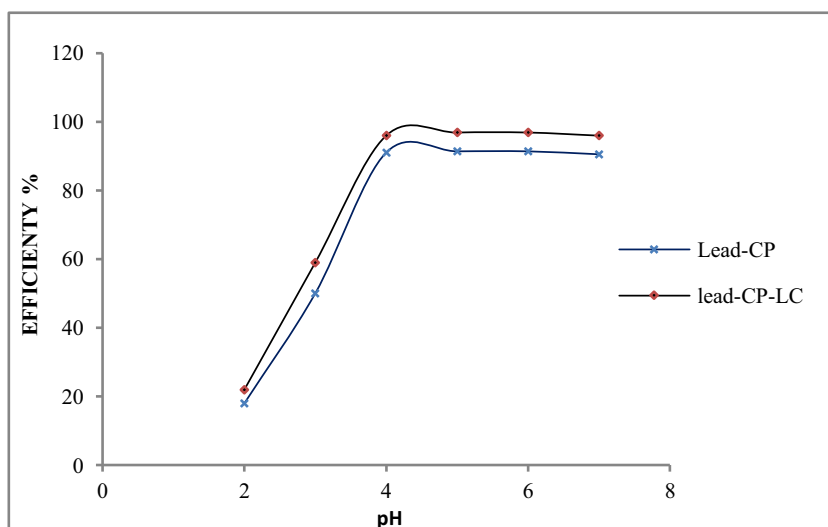


Fig. 3 Effect of initial pH of the solution on the biosorption of Pb (II) by CP and CP-LC. (initial concentration 10 mg/L; contact time: 40 min; biosorbent dose: 1 g/L; temperature: 298 K)

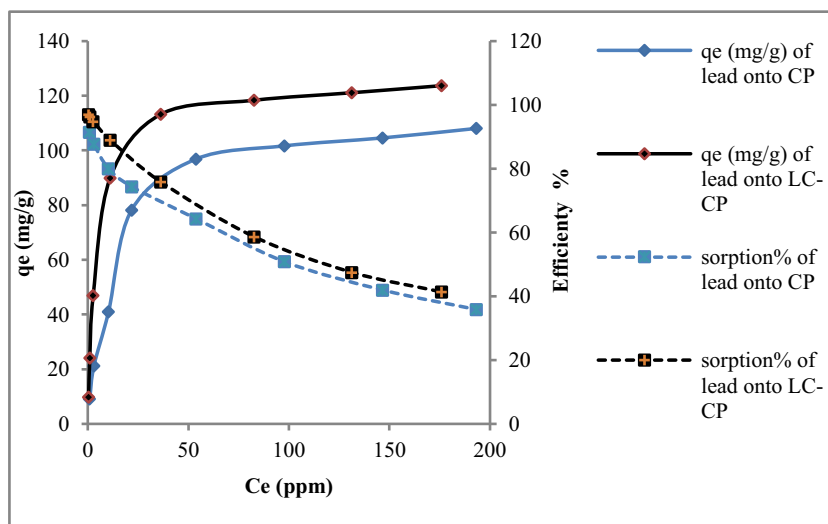


In the overall equations, M represents the Pb (II) ions and R represents the matrix of CP or CP-LC. Attempt to elevate the pH above pH 6 resulted in the precipitation of lead (II) ions out of solution; thus, pH 5 was taken as the optimum pH for the biosorption of Pb (II) onto CP and CP-LC.

4.3 Effect of initial concentration

Lead solutions with different initial concentrations in the range of 10–300 mg/L at 298 K and optimal pH 5 were equilibrated using 1-g biosorbent dose for both biomass CP and CP-LC. The analysis of the current results of metal ion biosorption demonstrated that the biosorption capability of sorbents was affected by the level of initial concentrations. Figure 4 shows

Fig. 4 Effect of the initial concentration of Pb (II) biosorption onto CP and CP-LC (pH 5.0, time 40 min., temp. 298 K)



that the Pb (II) ion equilibrium biosorption capacity onto free and immobilized *C. pyrenoidosa* increases from 9.2 to 108.04 mg/L, 9.8 to 123 mg/L, and elimination rate decreases from 91.36 to 35.86% and 96.9 to 41.36%, respectively when its initial concentration increases from 10 to 300mg/L. At higher initial concentrations, the active site’s biomass surface would be surrounded with more metal ions in the solution; for that reason, the equilibrium adsorption capacity of the adsorbent increases with increasing the metal ions concentration which reinforces the adsorption process. In contrast, the removal efficiency decreases by an increase in metals’ initial concentration. At low initial concentrations, the rate of the initial number of metal ions to the accessible active sites of sorbents is low; as a result, the removal efficiency of metal ions is higher and at higher initial concentrations [23].

4.4 Biosorption kinetic

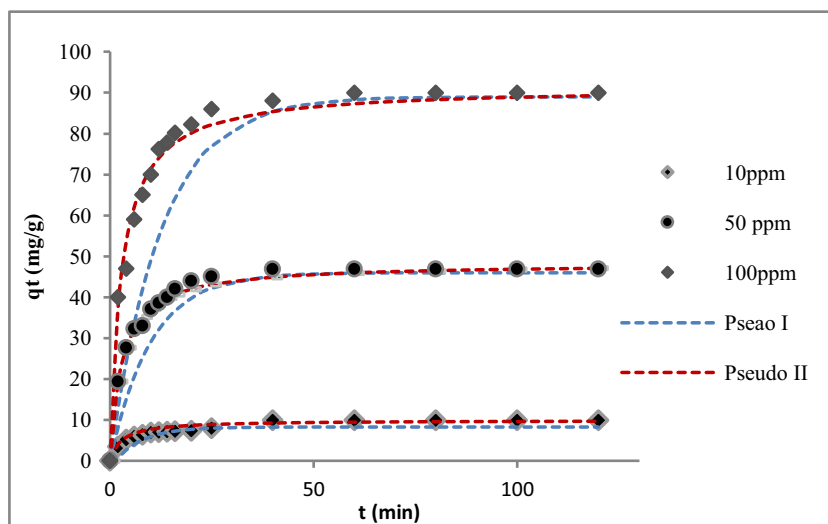
The effects of contact time and initial concentration of Pb (II) on the biosorption process were studied under the following conditions: time range from 5 to 120 min, pH 5.0, 298 K, and using different initial Pb (II) concentrations 10, 50, and 100 mg/L. For all Pb (II) concentrations studied, it was possible to show that an increase in contact time corresponds to an increase in amount biosorption capacity. The biosorption

increases quickly during the first 20 min, and after 40 min the adsorption remains constant. According to the results presented in Fig. 5, it is possible to verify that the time necessary to reach the equilibrium was 40 min. The result obtained from the experimental data was used to study the kinetics of lead ion biosorption. The rate kinetics of Pb (II) biosorption on the CP-LC was analyzed using pseudo-first-order and pseudo-second-order models. The kinetic parameters for different Pb (II) initial concentrations are presented in Table 3. Plots of pseudo-first-order and pseudo-second-order kinetic models are shown in Fig. 5. As shown in Table 4, the coefficients of determination (R^2) calculated from the plots of pseudo-second-order kinetic models were higher ($R^2 > 0.999$) than those of the pseudo-first-order models for all studied initial Pb (II) concentration. However, the values of ARE determined from the pseudo-second-order kinetic model were much lower than that of the pseudo-first-order models. The value of ARE relates to the conformity between the model-predicted and the experimental data values. In general, the lower the ARE values, the greater is the conformity effect. In contrast, the calculated values of $q_{e,cal}$ determined from the pseudo-second-order equation perfectly agreed with the experimental points of $q_{e,exp}$ at all initial concentrations. These results revealed that the pseudo-second-order fits the experimental data better than the pseudo-first-order model. It

Table 3 Kinetic parameters of Pb (II) biosorption by CP-LC

Pb (II) concentration. (mg/L)	$q_{e,exp}$	Pseudo-first order				Pseudo-second order				
		$q_{e,cal}$ (mg/g)	k_1 (1/min)	R^2	ARE	$q_{e,cal}$ (mg/g)	k_2 (g/(mg/min))	h_0	R^2	ARE
10	9.89	8.93	0.144	0.970	7.18	10.00	0.035	3.5	0.999	2.16
50	46.6	40.73	0.100	0.970	10.88	47.05	0.071	16	0.999	1.9
100	89.9	70.99	0.08	0.93	21.16	93.03	0.036	36	0.999	1.6

Fig. 5 Adsorption kinetic models of Pb (II) by CP-LC.



can also be seen in Table 3 that, with an increase in initial Pb (II) concentration, the initial biosorption rate (h_0) increased from 3.5 to 36 mg/g as the initial metal concentration increased from 10 to 100 mg/L. This may be due to the increase of driving force between the solute sorbate and adsorbent molecules with the increasing lead (II) concentration. In contrast, the rate constant (k_2) of the pseudo-second-order model presented the opposite trend.

4.5 Isotherm models

At explicit conditions, each adsorption system tends to control a dynamic equilibrium between the solute sorbate located on the internal surface of the biomass and the equilibrium concentration of sorbate in the solution. Adsorption isotherm models describe the relationship between the sorption capabilities of molecules removed from the solution by a unit mass of adsorbent at a constant temperature ($T = \text{const}$). The parameters of isotherms often give useful information on the adsorption mechanism, surface characteristics affinity of the sorbent. It is necessary to emphasize the determination of the most suitable correlation of equilibrium curves for optimizing the conditions for designing the adsorption process. In this study, eighteen models of mono- and multi-parameter are examined to analyze the experimental data.

4.5.1 One- and two-parameter models

Henry's Isotherm model [11] is considered the simplest adsorption isotherm model with one parametric linear regression model available at a low concentration of sorbate without regard to the surface of coverage in which all the adsorbate molecules are secluded from their closest neighbors. The Langmuir model [12] is used to

describe the adsorption of dissolved molecules in solution. This empirical isotherm supposes that the sorption is limited to monolayer; once a molecule of adsorbate occupies a single layer, the theory of Langmuir assumes that the adsorbent surface is homogeneous and sorption activation energy is uniform for all sites of sorbent and there is no movement of adsorbates in the plane of the surface. There is no interaction between adsorbate molecules on neighboring sites. The Freundlich model [11] defines the reversible and non-ideal adsorption process and is not restricted to the monolayer sorption in which its application to the multilayer formation is possible with a non-uniform distribution for adsorption heat and affinity over a heterogeneous surface. The Elovich model [12] is based on kinetic development and supposing that the multilayer formation increases exponentially with the adsorption site. The Temkin model [11] takes into consideration the effects of indirect adsorbent-adsorbate interactive relation on adsorption, and due to these interactions, the heat of the adsorbent of all the molecules in the surface decreases linearly as a result of increased surface coverage. This model presumes that adsorption heat (ΔH_{ads}) as a function of temperature, of all adsorbed molecules existing in the layer, declines linearly rather than logarithmically due to the surface coverage increase. The Fowler–Guggenheim model [12] is one of the simplest isotherms allowing for the lateral interaction of adsorbed molecules. If the interaction among adsorbate molecules is attractive, this means that the heat during adsorption will increase with loading; this is due to the fact that the increased interaction between adsorbed molecules as the loading increases (that is W is positive) the heat. However, the interaction between adsorbate molecules is repulsive and that is due to the heat during

Table 4 Isotherm constants of two-parameter models for Pb (II) biosorption onto CP and CP-LC

Isotherm model	parameters	CP	CP-LC	
Henry model	K	0.745	0.933	
	R ²	0.800	0.700	
	S ²	1532.84	2624.21	
	ARE	58.54	64.44	
	ERSQ	10766.94	18579.49	
	HYBRID	1086.40	37043.96	
	MPSED	62.00	178.09	
Henry’s law (Linear with intercept)	A	0.446	0.529	
	B	40.65	51.72	
	R ²	0.808	0.764	
	S ²	562.64	2228.89	
	ARE	68.54	92.73	
	ERSQ	3939.94	15602.24	
	HYBRID	1055.40	1833.52	
	MPSED	4.62	4.71	
	Langmuir	q _{mas} (mg/g)	114.94	126.58
		K _L (L/mg)	0.079	0.324
R ²		0.983	0.981	
S ²		167.69	150.16	
ARE		14.52	13.81	
ERSQ		1183.18	1065.97	
HYBRID		249.03	216.68	
MPSED		1.86	1.90	
Freundlich		K _F (mg/g)(L/mg) ^{1/n}	12.787	24.090
		n	2.19	2.69
	R ²	0.924	0.93	
	S ²	422.69	400.05	
	ARE	18.10	19.10	
	ERSQ	2536.15	1999.38	
	HYBRID	489.63	470.1	
	MPSED	2.74	2.81	
	Elovich	q _{Me} (mg/g)	39.680	32.154
		K _F (L/mg)	0.341	1.896
R ²		0.826	0.783	
S ²		1343.81	3344.10	
ARE		26.29	39.34	
ERSQ		8063.28	20064.91	
HYBRID		1739.56	2810.75	
MPSED		4.75	6.40	
Temkin		A _T (L/g)	1.352	5.302
		b _T (Kj/mol)	1.21	0.78
	R ²	0.979	0.97	
	S ²	77.44	170.3	
	ARE	19.96	19.16	
	ERSQ	464.69	722.25	
	HYBRID	298.56	191.06	
	MPSED	7.47	2.24	
	Fowler–Guggenheim	W (Kj/mol)	68.210	66.83
		K _{FG} (L/g)	1.720	K _{FG} =3.67
R ²		0.894	0.971	
S ²		626.38	672.15	
ARE		28.309	74.10	
ERSQ		3.77	4032.90	
HYBRID		1234.74	1093.27	
MPSED		6.35	4.14	
Kiselev		K ₁ (L/g)	0.102	0.2834
		K ₂	-0.965	-0.4297
	R ²	0.864	0.880	
	S ²	1069.89	1720.99	
	ARE	32.46	83.68	
	ERSQ	6419.36	10325.96	
	HYBRID	2573.89	1828.66	
	MPSED	8.80	4.86	
	Hill–de Boer	K _H (L/g)	0.054	0.172
		K _n (Kj/mol)	-80.729	-88.68

Table 4 (continued)

Isotherm model	parameters	CP	CP-LC
Flory–Huggins	R^2	0.828	0.794
	S^2	774.08	1365.30
	ARE	37.48	37.23
	ERSQ	3639.67	8191.81
	HYBRID	1449.43	4022.76
	MPSED	6.07	12.43
	n_{FH}	0.305	0.220
	K_{FH} (L/g)	0.00085	0.00084
	R^2	0.95	0.98
	S^2	119.37	122.73
	ARE	26.38	14.26
	ERSQ	1219.23	1136.42
	HYBRID	127.52	136.21
	MPSED	1.67	1.83

adsorption showing a decrease with loading (that is W is negative). When there is no interaction between adsorbed molecules (that is $W = 0$), this Fowler–Guggenheim isotherm will reduce to the Langmuir equation. The Kiselev isotherm model [12] is used to explain the localized monomolecular layer formation of adsorbate on adsorbents at equilibrium and this model is valid when surface coverage is greater than 0.68. The Hill-de Boer adsorption model [11] describes the mobile adsorption and lateral interaction among adsorbed molecules. The apparent affinity is increased with loading when there exists an attraction between adsorbed species (that is K_n is positive) and it is decreased with loading when there is repulsion among the adsorbed species (that is K_n is negative). The Flory-Huggins isotherm [11, 12] is used for understanding the nature of the surface coverage degree of the adsorbate on the adsorbent. This model describes the nature of the adsorption process in regard to the feasibility and spontaneity of the process.

Equilibrium tests were performed under optimum conditions obtained from the model predicted. Constants and parameters of the adsorption isotherm models as well as their associated percentage error values are listed in Table 4. As shown in Table 4, Henry's isotherm model completely fails to predict the experimental data due to poor results showed in R^2 and error function values for both CP and CP-LC. This could be due to the unavailability of sorption data in the low sorbate concentrations. In a liquid-phase sorption system, the equilibrium data are commonly obtained at higher concentrations, where the sorbent surfaces are almost on the verge of saturation sites. Hence, this study supports the fact of the failure of Henry's model at the higher sorbate concentration range. Furthermore, high residual concentrations may suggest the applicability of an isotherm model with a linear regression between q_e and C_e at the final part of the

experimental data. This requirement could be partly fulfilled by applying Henry's law model (linear with intercept). The addition of a constant term in Henry's model reveals the model combines the basic characteristics of the experimental data at the high-level concentration. A comparison of regression constants provided the improvement in R^2 , S^2 , ARE, ERSQ, HYBRID, and MPSED values by Linear with intercept over Henry's model. The addition of the parameter in the model ameliorates the capability of modeling the equilibrium data. However, the applicability of the other two-parameter isotherm models was studied. Isotherm model plots for removal of Pb (II) onto CP and CP-LC are shown in Fig. 6. According to Table 4, experimental data are fitted better by the Langmuir model compared to other isotherm models. Moreover, the accuracy analysis of the Langmuir, Freundlich, Temkin, Elovich, Fowler-Guggenheim, Kiselev, Hill de Boer, and Flory-Huggins models was evaluated by the statistics of R^2 , S^2 , ARE, ERSQ, HYBRID, and MPSED. By comparisons with other isotherm models, the high R^2 (0.983 and 0.981 for CP and CP-LC, respectively) as well as the low S^2 (167.69 and 150.16 for CP and CP-LC, respectively), ARE (14.52 and 13.81 for CP and CP-LC, respectively), ERSQ (1183.18 and 1065.97 for CP and CP-LC, respectively), HYBRID, and MPSED (1.86 and 1.90 for CP and CP-LC, respectively) values confirm that the Langmuir model is more fitted to the experimental data obtained (Table 4). This result elucidates that the process of adsorption proceeds as a monolayer on uniform surfaces. The maximum biosorption capacities for Pb (II) onto CP and CP-LC are 114.94 and 126.58 mg/g, respectively. The Langmuir constant value K_L which is attributed to the binding energy of the active site of biosorbents with lead ions onto CP and LC is 0.079 and 0.324 L/g, respectively. The most important characteristics of the Langmuir isotherm parameter can be used to evaluate the affinity

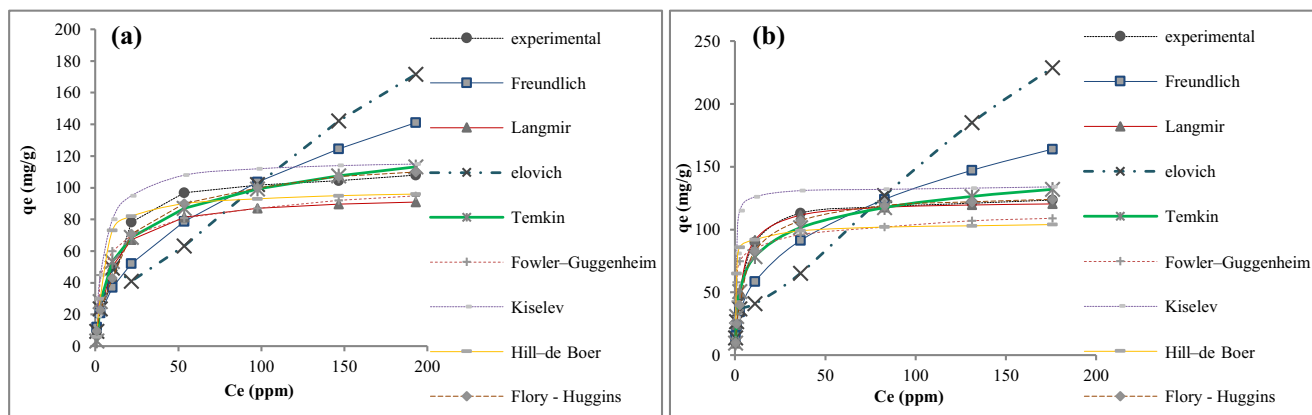


Fig. 6 Comparative non-linear plots for eight two-parameter isotherm models; **a** biosorption of Pb (II) onto CP, **b** biosorption of Pb(II) onto CP-LC

between the sorbate and sorbent using dimensionless equilibrium parameter or separation factor. The value of dimensionless equilibrium parameter R_L revealed important information about the nature of adsorption. The values of R_L vs initial Pb (II) concentrations between 10 and 300 mg/L are 0.55–0.04, 0.23–0.01 for CP and CP-LC, respectively. These results indicated that the sorption process is favorable and reversible, because $0 < R_L < 1$ [12]. Unlike the Langmuir model, the Elovich model exhibited lower coefficients of determination R^2 (0.826 and 0.783 for CP and CP-LC, respectively) as well as high S^2 (1343.81 and 3344.10 for CP and CP-LC, respectively), ARE (26.29 and 39.34 for CP and CP-LC, respectively), ERSQ (8063.28 and 20064.91 for CP and CP-LC, respectively), HYBRID (1739.56 and 2810.75 for CP and CP-LC, respectively), and MPSED (4.75 and 6.40 for CP and CP-LC, respectively) values. Furthermore, the values of maximum biosorption capacity obtained for CP and CP-LC were very lower than the experimental quantity of the sorbate on the biosorbent in the equilibrium state uptake corresponding to the plateaus of the adsorption isotherm. This is maybe due to the fact this isotherm model describes the multilayer sorption process indicating migration between layers. For this reason, the Elovich model is inefficient to describe the biosorption isotherms of Pb (II) onto free and immobilized *C. pyrenoidosa*. The n value (Freundlich model constant) indicates the factor of non-linearity between sorbate concentration and adsorption as follows: if $n < 1$, then adsorption is a chemical process; if $n > 1$, then adsorption is a physical process; if $n = 1$, then adsorption is linear [24, 25]. The n value in the Freundlich model was found to be 2.19 and 2.69 for CP and CP-LC, respectively. Since n falling between 1 and 10, this is due to the physical biosorption of lead (II) onto CP and CP-LC. The variation of adsorption energy $b_T = (-\Delta H)$ in the Temkin isotherm model was found to be 1.21 and 0.78 KJ/mol for CP and CP-LC,

respectively. Since the positive value of the variation indicates that the adsorption of Pb (II) onto the CP and CP-LC is exothermic in nature, additionally, the low $b_T < 8$ values confirm that the interactions between the lead molecules and the biosorbents are weak and the adsorption mechanism of lead ions can be expressed as physisorption [26]. Moreover, it was observed that the W values > 0 (Fowler–Guggenheim model constant) and the K_n values < 0 (Hill–de Boer model constant) for the removal of Pb (II) on CP and CP-LC, which validate the repulsion between the adsorbed molecules, were $w = 68.210$ and 66.83 KJ/mol for CP and CP-LC, respectively and $K_n = -80.72$ and -88.66 KJ/mol for CP and CP-LC, respectively [12]. On the other hand, the values of K_{FH} (Flory-Huggins model constants) were found to be 0.00085 and 0.00084 KJ/mol for CP and CP-LC, respectively. These positive values indicate negative Gibbs free energy ($\Delta G = -RT \ln K_{FH}$); for that reason, the spontaneity of the sorption process stems from high Pb (II) occupancy of the CP and CP-LC surfaces. The results of the Flory model also reveal that the number of adsorbate molecules occupying adsorption sites ($n_{FH} < 1$) indicates grander than the unity active zone of adsorbent materials that would be occupied by adsorbate molecules [11]. In the case of the Kiselev model, the equilibrium parameter of the formation of the complex between adsorbed compounds, k_n values, is negative for both biosorbents, which is surprising because it is an equilibrium parameter and it should be positive. Having negative values of k_n (L/mg) elucidates that there is no formation of the complex between the biosorbed molecules.

4.5.2 Three-parameter models

The abilities of the three parameter models, Redlich-Peterson, Sips, Koble–Carrigan, Radke-Prausnitz, Toth, and Khan models, to model the experimental biosorption data were

tested. All these models have been derived from the Langmuir and Freundlich models. The Redlich–Peterson isotherm [11] combines the features of these two models, and the mechanism of the adsorption process is a hybrid and does not follow ideal monolayer adsorption. This isotherm can be applied for both homogeneous and heterogeneous systems. Sips isotherm [11, 12] proposed an expression that combines the Freundlich and Langmuir models. This produces an equation that exhibits a finite limit at sufficiently high concentration. This isotherm is available for predicting the heterogeneous adsorption process and localized adsorption without interaction between adsorbate/adsorbate. The Koble–Corrigan model [12] is generally applied for the heterogeneous adsorbent surface. This model is valid only when $n_K > 1$ that is due to the model which is able to describe the experimental data. Radke–Prausnitz isotherm [12] is a simple yet powerful mathematical model for most adsorption systems at low adsorbate concentrations; this model reduces to a linear isotherm, while at high sorbate concentration, it becomes the Freundlich model and when it becomes the Langmuir isotherm. Another characteristic of this isotherm is that it gives the best fit over a wide range of sorbate concentrations. Toth isotherm [11, 18] is an empirical modified form of the Langmuir expression, aiming to reduce the error between the value of both the experimental and predicted points. Mainly, this isotherm is used for the description of the heterogeneous adsorption process, satisfying the low and high concentration of sorbate. Khan isotherm [12] is a generalized model suggested for the adsorbate adsorption from pure dilute equation solutions development of this model was made for both single and multicomponent adsorption.

The equilibrium data were examined according to the non-linear regression of three-parameter models. Table 5 shows the isotherms parameters and worse fits of CP and CP-LC. The prediction of adsorption isotherms of Pb (II) onto CP and CP-LC is shown in Fig. 7. From the analysis of all tested isotherm models of three parameters and based on the error values, the isotherm model can be arranged according to their efficiency in predicting the equilibrium data. For Pb (II)-CP system: Sips > Radke–Prausnitz > Toth > Khan > Koble–Carrigan > Redlich–Peterson. In the case of Pb (II)-CP-LC system: Koble–Carrigan > Radke–Prausnitz > Khan > Sips > Redlich–Peterson > Toth. The values of g (Redlich–Peterson model constant), n_s (Sips model constant), n_R (Radke–Prausnitz model constant), n_T (Toth model constant), and a_K (Khan model constant) obtained using Redlich–Peterson, Sips, Toth, Radke–Prausnitz, and Khan models are near than unity, which means that the adsorption processes reduce to the Langmuir isotherm. This implies that the adsorption already predicted to be on homogeneous surfaces is also confirmed by the Koble–Corrigan isotherm model. This model defines the validity or otherwise of a system. $n_K \geq 1$ implies a valid adsorption system, while $n_K \leq 1$ signifies the models' inefficiency in defining the experimental data, despite the

Table 5 Isotherm constants of three-parameter models for Pb (II) biosorption onto CP and CP-LC

Isotherm model	Parameters	CP	CP-LC
Redlich–Peterson	K_R (L/g)	18	$K_R = 35$
	a_R (L/g)	0.682	$a_R = 0.4$
	b_R	0.690	$b_R = 0.9$
	R^2	0.955	0.990
	S^2	251.24	69.16
	ARE	16.93	6.51
	ERSQ	1256.12	334.83
	HYBRID	289.36	75.33
	MPSED	1.95	0.90
Sips	q_{ms} (mg/g)	117.1	123
	K_s (L/g)	0.086	0.2
	n_s	1.059	1.1
	R^2	0.992	0.980
	S^2	37.71	86.78
	ARE	7.16	11.96
	ERSQ	193.58	434.94
	HYBRID	61.878	135.28
	MPSED	1.13	1.95
Koble–Carrigan	A_K (L/g)	11.60	35
	B_K (L/g)	0.11	0.3
	n_K	1.02	1.1
	R^2	0.987	0.992
	S^2	82.82	42.33
	ARE	11.77	6.06
	ERSQ	414.14	211.66
	HYBRID	137.56	60.83
	MPSED	1.62	0.5
Radke–Prausnitz	q_m (mg/g)	333.33	308.33
	K_{RP} (L/g)	0.0187	0.93
	n_R	1.2	1.1
	R^2	0.994	0.992
	S^2	37.9	45.67
	ARE	7.52	6.12
	ERSQ	182.89	228.35
	HYBRID	64.39	67.48
	MPSED	1.13	0.51
Toth	q_{mK} (mg/g)	118	123
	k_L (L/g)	0.096	0.264
	n_T	0.90	0.95
	R^2	0.991	0.98
	S^2	38.435	324.49
	ARE	8.95	19.95
	ERSQ	269.04	1123.91
	HYBRID	65.63	412.45
	MPSED	1.13	3.34
Khan	q_{mKH} (mg/g)	107	121.84
	b_{KH} (L/g)	0.091	0.4
	a_{KH}	0.95	0.97
	R^2	0.991	0.993
	S^2	39.58	54.75
	ARE	9.97	6.36
	ERSQ	187.93	233.78
	HYBRID	68.066	69.75
	MPSED	1.50	0.57

results from other goodness-of-fit adjudging criteria (correlation coefficient or low error value). This is due to the fact this isotherm model describes the heterogeneous surface.

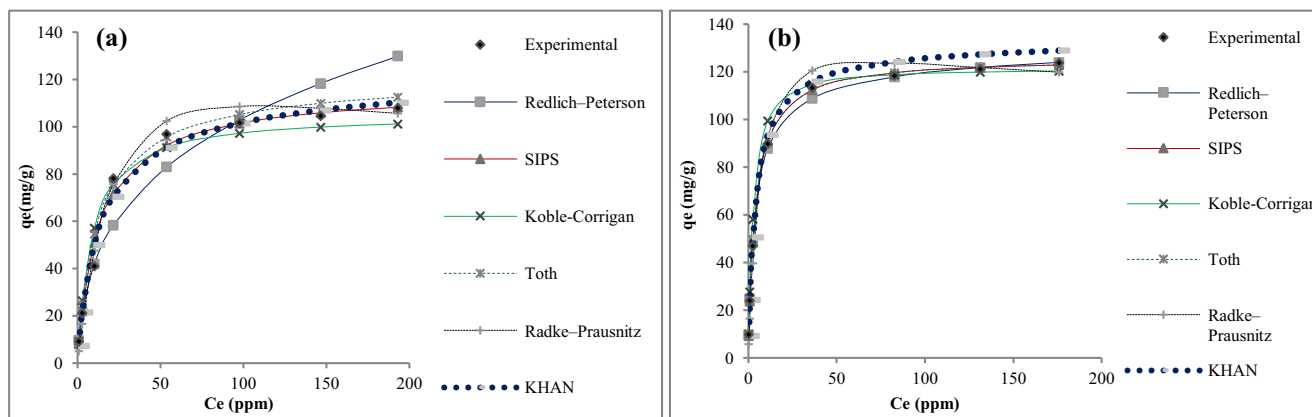


Fig. 7 Comparative non-linear plots for six three-parameter isotherm models; **a** biosorption of Pb (II) onto CP, **b** biosorption of Pb (II) onto CP-LC

4.5.3 Four- and five-parameter models

Among the four- and five-parameter models considered in the present study to model the experimental data are Baudu, Fritz-Schlünder model (IV), and Fritz-Schlünder model (V). The Baudu model [11] has been developed mainly due to the arise of discrepancy in determining the Langmuir parameters and coefficient from the slope of tangent over a wide concentration range. This isotherm is valid in the range of $(1+x+y) < 1$ and $(1+x) < 1$. Fritz-Schlünder model (IV) Fritz-Schlünder model and (V) [12] are developed for the aim of simulating the model variations more accurately for application over a wide range of excremental data. The equilibrium data were modeled according to the nonlinear regression of the four and five parameter models. Figure 8 depicts the predict curves of four and five parameter isotherm for CP and CP-LC.

Analyzing the results of the four- and five-parameter models represented in Table 8, it can be observed that the Fritz-Schlünder (V) isotherm model is the best to fit the experimental data of Pb (II) biosorption onto both CP and CP-LC. Indeed, this isotherm model shows relatively high error values R^2 (0.996 and 0.997 for CP and CP-LC, respectively)

and the lowest other error function values S^2 (27.40 and 10.40 for CP and CP-LC, respectively), ARE (5.00 and 2.53 for CP and CP-LC, respectively), ERSQ (137.02 and 50.02 for CP and CP-LC, respectively), HYBRID (47.71 and 11.68 for CP and CP-LC, respectively), and MPSED (0.75 and 0.44 for CP and CP-LC, respectively). This improvement is due to the increase in the number of constants, which can perform a more accurate simulation of model variations for representation over a wide range of experimental results. Based on that, and in order to give goodness of fit to the experimental data, we have modified the equation of the Fritz-Schlünder (V) model. For this reason, we propose to introduce other constants which improved the fit of experimental data. The formula of the modified Fritz-Schlünder (V) model (seven parameters) that we have developed is expressed as follows:

$$q_e = \frac{q_{mFSS}K_{FS1}C_e^{M1} + \alpha}{1 + (K_{FS2}C_e^{M2} + \beta)} \tag{10}$$

The constants α and β are considered the correction coefficients. These coefficients are added to the equation of the Fritz-Schlünder (V) that take into consideration the

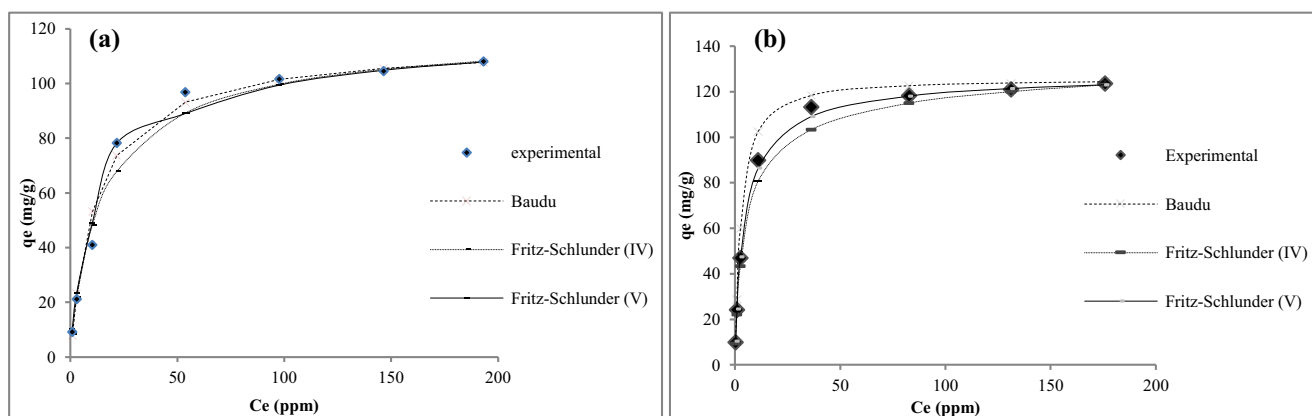


Fig. 8 Comparative non-linear plots of four and five parameter isotherm models; **a** biosorption of Pb (II) onto CP, **b** biosorption of Pb (II) onto CP-LC

experiment errors. K_{FS1} and K_{FS2} are the modified Schlünder (V) model parameters; M_1 and M_2 are the exponents of the modified First-Schlünder (V) equation. According to Table 6, it is evident that the R^2 values have increased and error values decreased by using the modified First-Schlünder (V) equation, and the values of error functions are reduced compared to that of all other models studied for biosorption of Pb (II) onto CP and CP-LC. Figure 9 shows the curves of the nonlinear regression of experimental data as well as the modified Schlünder (V) for CP and CP-LC. As observed, the curve of the nonlinear regression of the modified First-Schlünder (V) equation depicts a good approximation between experimental and predicted data compared to the other model. Therefore, the m Fritz-Schlünder (V) model shows a better representation of these experimental data.

4.6 Thermodynamic parameters

In order to estimate the effect of temperature on the biosorption of Pb (II) onto CP-LC, the process was carried out at several temperatures ranging from 298 to 318 K with 100 mg/L of initial Pb (II) concentrations at pH 5.0. The equilibrium lead ion biosorption capacity of the CP-LC was better at lower temperatures as the adsorbed amount of lead ions decreased with the rise in temperature. It is important to mention that the bio-adsorption process is usually not functioned at high temperatures [27]. Since bio-adsorption reactions are normally exothermic, the decrease in biosorption capacity between 298 and 343K may be due to the damage of active sites in the immobilized *C. pyrenoidosa* in *Luffa cylindrica*. Temperature dependence of the bio-adsorption process is related to the three thermodynamic parameters namely enthalpy (ΔH°), entropy (ΔS°), and free energy change (ΔG°), which are used to determine whether the biosorption process is spontaneous or not. Thermodynamic parameters can be obtained from the following equation [25]:

$$\Delta G^0 = -RT \ln K_c \quad (11)$$

$$\ln K_c = \frac{\Delta S^0}{R} - \frac{\Delta H^0}{RT} \quad (12)$$

$$\Delta G^0 = \Delta H^0 - T \Delta S^0 \quad (13)$$

$$K_c = \frac{as}{ae} = \frac{Y_s}{Y_e} = \frac{C_s}{C_e} \quad (14)$$

where K_c is the distribution constant, as is the activity of adsorbed Pb (II), ae is the activity of Pb (II) in solution at equilibrium, Y_s is the activity coefficient of adsorbed Pb (II), Y_e is the activity coefficient of Pb (II) in equilibrium solution, C_s is Pb (II) adsorbed on CP-LC (mg/g), and C_e is Pb (II) concentration in equilibrium solution (mg/L). (ΔH°), (ΔS°), and (ΔG°) are enthalpy (kJ/mol), entropy (J/mol K), and change in Gibbs free energy (kJ/mol), respectively. R is the

Table 6 Isotherm constants of multi-parameter models for Pb (II) biosorption onto CP and CP-LC

Isotherm model	Parameters	CP	CP-LC	
Baudu	q_{mb} (mg/g)	108	125	
	b_0 (L/g)	0.09	0.32	
	X	0.001	0.001	
	Y	0.1	0.1	
	R^2	0.992	0.994	
	S^2	37.28	78.9	
	ARE	8.00	9.08	
	ERSQ	186	394.53	
	HYBRID	71.5	108.27	
	MPSED	1.37	1.33	
	Fritz-Schlunder (IV)	C (L/g)	10	29.5
		D (L/g)	0.09	0.25
		M_1	0.95	0.9
M_2		0.881	0.89	
R^2		0.995	0.996	
S^2		43.38	51.38	
ARE		6.89	6.77	
ERSQ		218	295.83	
HYBRID		68.67	71.77	
MPSED		1.10	1.12	
Fritz-Schlunder (V)		q_{MFS} (mg/g)	108	123
		K_{FS1} (L/g)	0.094	0.26
		K_{FS2} (L/g)	0.0881	0.25
	M_1	0.95	0.9	
	M_2	0.881	0.89	
	R^2	0.996	0.997	
	S^2	27.40	10.40	
	ARE	5.00	2.35	
	ERSQ	137.02	50.02	
	HYBRID	47.71	11.68	
	MPSED	0.75	0.44	
	Modified-Schlunder (V)	q_{Mfs} (mg/g)	108	123
		K_{FS1} (L/g)	0.094	0.26
K_{FS2} (L/g)		0.0881	0.25	
M_1		0.95	0.95	
M_2		0.881	0.881	
α		0.99	-1	
β		0.00	0.1	
R^2		0.999	0.999	
S^2		4.20	7.62	
ARE		2.50	2.26	
ERSQ		21.25	38.02	
HYBRID		9.5	8.61	
MPSED		0.49	0.3	

universal gas constant (8.314 J/mol K) and T is the temperature in Kelvin. Values of the standard Gibbs free energy change (ΔG°) for the biosorption process are listed in Table 7. Gibbs free energy change (ΔG°) was found to be -10.64 , -11.09 , -11.24 , -11.40 , and -11.50 kJ/mol at 298, 303, 308, 313, and 318 K, respectively. The negative values of ΔG° indicated the spontaneous nature of the process and its feasibility for the temperature range were evaluated.

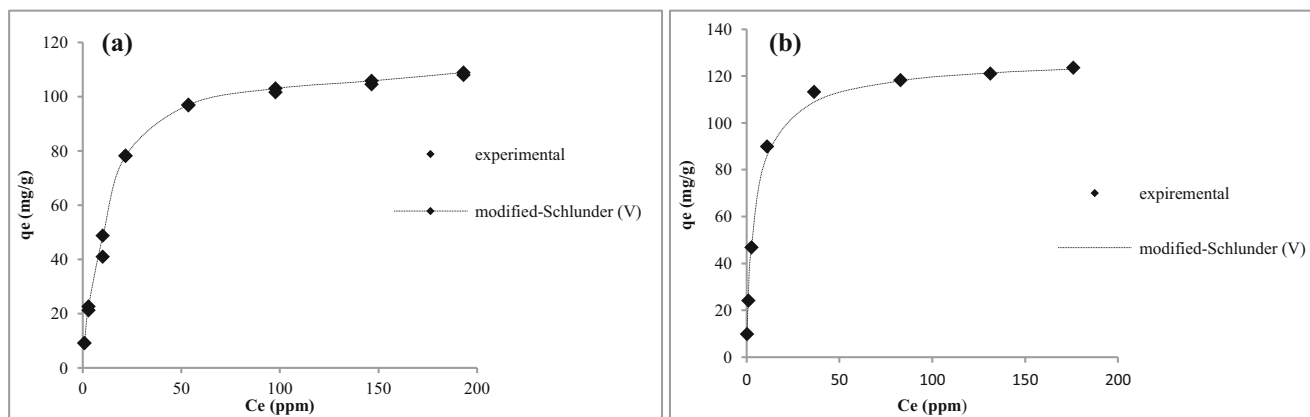


Fig. 9 Non-linear isotherm representations of modified Schlünder (V); **a** biosorption of Pb (II) onto CP, **b** biosorption of Pb (II) onto CP-LC

Table 7 Thermodynamic parameters of Pb (II) biosorption onto CP-LC at different T

Temperature (K)	ΔG° (kJ/mol)	ΔH° (kJ/mol)	ΔS° (K J/mol.K)
298	-10.64	-1.70	+0.031
303	-11.09		
308	-11.24		
313	-11.40		
318	-11.50		

Moreover, the increase in temperature resulted in a decrease in Gibbs free energy, suggesting that better adsorption is actually obtained at lower temperatures. The negative value observed for ΔH° (-1.70 kJ/mol) indicates an exothermic process and the positive values of ΔS° (0.031 kJ mol. K) was not very large and indicated increased randomness at the solid/solution interface during the biosorption of lead ions and good affinity of Pb (II) towards CP-LC. Some researchers have indicated that the positive values of ΔS° reflected some structural changed in the sorbent [28].

4.7 Regeneration study

For wide-scale applications, reusability and regeneration are the vital biosorbent properties, since the ability to reutilize a biosorbent is a crucial factor for the decontamination

operation from the economic point of view. The desorption experiments presented in Fig. 10 show that the H_2SO_4 and HCl recovered about 99% and 95% of Pb (II) adsorbed on the biosorbent surface, respectively. Tap water, de-ionized water, and NaOH indicated a low desorption ratio of 14.04%, 30.07%, and 49.5% of Pb (II) adsorbed on the immobilized *C. pyrenoidosa* surface, respectively. The study indicated that Pb (II) ions accumulated onto the CP-LC could be desorbed, and maximum ratio recovery of Pb (II) ions was 99% with 0.1 M H_2SO_4 . The hydroxyl and carboxylic groups in the CP-LC made it amenable to easy regeneration and desorption with the acid solutions [13]. Therefore, sulfuric acid solutions were selected as desorption reagents for removing Pb (II) ions from the immobilized *C. pyrenoidosa* surface. According to Table 8, the results for the adsorption/desorption cycle elucidated that CP-LC could be reused up to five times without significant change. Therefore, the prospects of CP-LC are good for practical applications of removing lead ions from queues solutions.

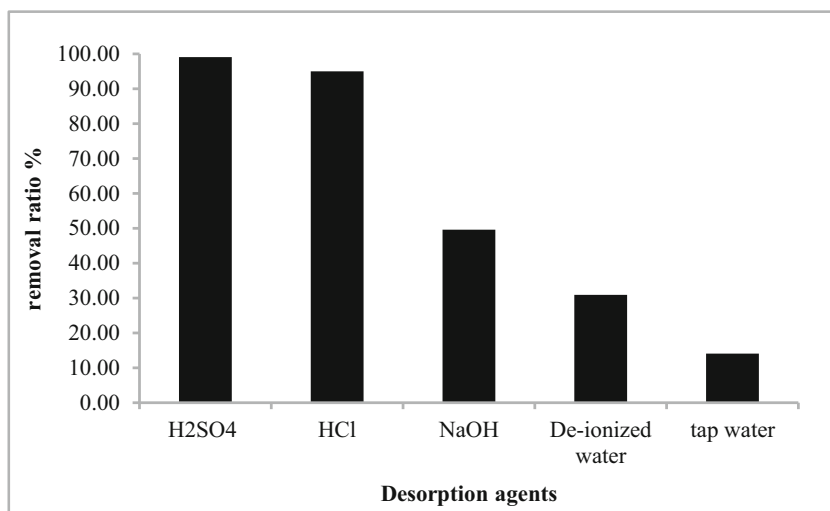
4.8 Comparison of immobilized *C. pyrenoidosa* with other biosorbents

The biosorption removal capacities of different biosorbents towards lead ions as documented in the literature are mentioned in Table 9. A comparison between this research and other documented data from the literature [29–37] elucidates

Table 8 Adsorption, desorption, and desorption/ reloading ratio of Pb (II) in five seductive cycles

Number of cycles	Adsorption (mg/g)	Desorption (mg/g)	Desorption ratio %	Reloading ratio %
1	9.96	9.95	99.98	-
2	9.81	9.72	99.00	98.50
3	9.77	9.73	99.59	98.09
4	9.69	9.67	99.79	97.28
5	9.62	9.48	98.54	96.58

Fig. 10 Desorption of Pb (II) ions adsorbed on CP-LC



that CP-LC a better biosorbent for Pb (II) compared to other biosorbents. Thus, it could be concluded that the CP-LC biomass has a significant potential for the removal of lead ions from an aqueous solution.

5 Conclusion

The new biosorbent has been prepared by the immobilization of *Chlorella pyrenoidosa* in *Luffa cylindrica*. According to the experimental results, the optimum temperature of solution, pH, biosorbent concentration, contact time, and initial lead ion concentration were determined as 298 K, 5.0, 1 g/L, 40 min, and 300 mg/L, respectively. The maximum biosorbent capacity (q_e) and biosorption yield of Pb (II) were obtained found to be 123 mg/g and 41.36%, respectively, at the optimum conditions. The biosorption data were studied and

modeled using eighteen well-known isotherm models. From the analysis of all tested models and the knowledge of the most principal parameters (q_m , R^2 , and error values), the isotherm model shows that the goodness-of-fit was obtained using the five-parameter model of Fritz–Schlunder (V) compared to the other model. Taking into account the outcome two coefficients added to equation Fritz–Schlunder (V) for reducing the error between the experimental and predicts data, the results of the fulfillment of this new mathematical model have significantly improved an approximation of the experimental data than Fritz-Schlunder (V) isotherm. This study elucidates that the adjustment of more parameters provides a better fitting of the equilibrium isotherms. Finally, the results of this study show that *C. pyrenoidosa* immobilized in *Luffa cylindrica* may be used as a low-cost, eco-friendly, and effective biosorbent to remove lead ions from aqueous media. Further study could be conducted to investigate the feasibility

Table 9 Comparison of the maximum biosorption capacity of immobilized chlorella pyrenoidosa in *Luffa cylindrica* for Pb (II) with other biosorbents

Biosorbents	Q_{\max} (mg g/g)	Pb ²⁺ concentration (mg/L)	pH	Biosorbent dosage (g/L)	Contact time (min)	Temperature (C)	References
<i>Oryza sativa</i> L. husk	5.69	10–200	-	20.0	120	30.0	[29]
<i>Cladonia furcata</i>	12.30	10–400	5.0	8.0	60	20.0	[30]
	13.7	10–300	5.0	10.0	-	25.0	[31]
Almond shell	26.32	10–6	4.84	2.0	180	30.0	[32]
<i>Eichhornia crassipes</i>							
Pine bark	76.8	50–1000	5.0	5.0	240	40.0	[33]
Neem bark	83.33	5–100	5.0	7.5	60	30 ± 2.0	[34]
Sawdust	88.49	5–100	5.0	7.5	60	30.0 ± 2.0	[34]
Ponkan peel	112.1	1–15 (mM)	5.0	-	60	25.0	[35]
CP	108	10–300	5.0	1.0	15	25.0 ± 0.5	Present study
CP-LC	123	10–300	5.0	1.0	15	25.0 ± 0.5	Present study

of immobilized *C. pyrenoidosa* as a biosorbent for removing other toxic heavy metals and dyes.

Acknowledgements The authors (s) thank the anonymous reviewers for helping us to present this research in a more effective manner. The authors also are thankful to Mr. Ramzi Touchan, Research Professor at the Laboratory of Tree-Ring Research, University of Arizona, for his critical suggestions.

Declarations

Conflict of interest The authors declare that they have no conflict of interest.

References

- Wei BG, Yang LS (2010) A review of heavy metal contaminations in urban soils, urban road dusts and agricultural soils from China. *Microchem J* 94:99–107. <https://doi.org/10.1016/j.microc.2009.09.014>
- Wang J, Chen C (2006) Biosorption of heavy metals by *Saccharomyces cerevisiae*: a review. *Biotechnol Adv* 24(5):427–451. <https://doi.org/10.1016/j.biotechadv.2006.03.001>
- Abhari PS, Manteghi F, Tehrani Z (2020) Adsorption of lead ions by a green AC/HKUST-1 nanocomposite. *Nanomaterials* 10(9):1647. <https://doi.org/10.3390/nano10091647>
- Agarwal A, Upadhyay U, Sreedhar I, Singh SA, Patel CM (2020) A review on valorization of biomass in heavy metal removal from wastewater. *J Water Process Eng* 38:101602. <https://doi.org/10.1016/j.jwpe.2020.101602>
- Moreira VR, Lebron YAR, Freire SJ, Santos LVS, Palladino F, Jacob RS (2019) Biosorption of copper ions from aqueous solution using *Chlorella pyrenoidosa*: optimization, equilibrium and kinetics studies. *Microchem J* 145:119–129. <https://doi.org/10.1016/j.microc.2018.10.027>
- Vidal CB, Melo DQ, Raulino GSC, da Luz AD, da Luz C, Nascimento RF (2016) Multielement adsorption of metal ions using Tururi fibers (*Manicaria saccifera*): experiments, mathematical modeling and numerical simulation. *Desalin Water Treat* 57(19):9001–9008. <https://doi.org/10.1080/19443994.2015.1025441>
- Kumar KV (2006) Comparative analysis of linear and non-linear method of estimating the sorption isotherm parameters for malachite green onto activated carbon. *J Hazard Mater* 136(21):197–202. <https://doi.org/10.1016/j.jhazmat.2005.09.018>
- Kumar KV, Porkodi K (2006) Relation between some two- and three-parameter isotherm models for the sorption of methylene blue onto lemon peel. *J Hazard Mater* 138:633–635
- Haloi N, Sarma HP, Chakravarty P (2013) Biosorption of lead (II) from water using heartwood charcoal of *Areca catechu*: equilibrium and kinetics studies. *Appl Water Sci* 3:559–565. <https://doi.org/10.1007/s13201-013-0112-3>
- Kuczajowska-Zadrozna M, Filipkowska U, Józwiak T (2020) Adsorption of Cu (II) and Cd (II) from aqueous solutions by chitosan immobilized in alginate beads. *J Environ Chem Eng* 8:103878. <https://doi.org/10.1016/j.jece.2020.103878>
- Al-Ghouti MA, Da'ana DA (2020) Guidelines for the use and interpretation of adsorption isotherm models: a review. *J Hazard Mater* 393:122383. <https://doi.org/10.1016/j.jhazmat.2020.122383>
- Rangabhashiyam S, Anu N, Giri Nandagopal MS, Selvaraju N (2014) Relevance of isotherm models in biosorption of pollutants by agricultural byproducts. *J Environ Chem Eng* 2(1):398–414. <https://doi.org/10.1016/j.jece.2014.01.014>
- Bayuo J, Abukari MA, Pelig-Ba KB (2020) Desorption of chromium (VI) and lead (II) ions and regeneration of the exhausted adsorbent. *Appl Water Sci* 10:171. <https://doi.org/10.1007/s13201-020-01250-y>
- Ding TY, Hii SL, Ong, L (2012) Ong, Comparison of pretreatment strategies for conversion of coconut husk fiber to fermentable sugars. *Bioresources* 7(2): 1540–1547. <https://doi.org/10.15376/biores.7.2.1540-1547>.
- Rescignano N, Fortunati E, Armentano I, Hernandez R, Mijangos C, Pasquino R, Kenny JM (2015) Use of alginate, chitosan and cellulose nanocrystals as emulsion stabilizers in the synthesis of biodegradable polymeric nanoparticles. *J Colloid Interface Sci* 445:31–39. <https://doi.org/10.1016/j.jcis.2014.12.032>
- Mitra T, Sailakshmi G, Gnanamani A, Mandal AB (2013) Studies on cross-linking of succinic acid with chitosan/collagen. *Mater Res* 16:755–765. <https://doi.org/10.1590/S1516-14392013005000059>
- Lim SH, Hudson SM (2004) Synthesis and antimicrobial activity of a water-soluble chitosan derivative with a fiber-reactive group. *Carbohydr Res* 339:313–319. <https://doi.org/10.1016/j.carres.2003.10.024>
- Bhattacharya A, Mathur M, Kumar P, Malik A (2019) Potential role of N-acetyl glucosamine in *Aspergillus fumigatus*-assisted *Chlorella pyrenoidosa* harvesting. *Biotechnol Biofuels* 12:178. <https://doi.org/10.1186/s13068-019-1519-3>
- Leal D, Matsuhira B, Rossi M, Caruso F (2008) FT-IR spectra of alginic acid block fractions in three species of brown seaweeds. *Carbohydr. Res*, 343(2): 308-316. <https://doi.org/10.1016/j.carres.2007.10.016>.
- Taşar Ş, Kaya F, Özer A (2014) Biosorption of lead(II) ions from aqueous solution by peanut shells: equilibrium, thermodynamic and kinetic studies. *Journal of Environmental Chemical Engineering*. *J Environ Chem Eng* 2(2):1018–1026. <https://doi.org/10.1016/j.jece.2014.03.015>
- Ozer A (2007) Removal of Pb(II) ions from aqueous solutions by sulphuric acid-treated wheat bran. *J Hazard Mater* 141(3):753–761. <https://doi.org/10.1016/j.jhazmat.2006.07.040>
- Adewuyi A, Pereira FV (2017) Underutilized *Luffa cylindrica* sponge: a local bio-adsorbent for the removal of Pb(II) pollutant from water system. *Beni Suef Univ J Basic Appl Sci* 6(2):118–126. <https://doi.org/10.1016/j.bjbas.2017.02.001>
- Karnib M, Kabbani A, Holail H, Olama, Z (2014) Heavy metals removal using activated carbon, silica and silica activated carbon composite. *Energy Procedia* 50: 113–120. doi: <https://doi.org/10.1016/j.egypro.2014.06.014>.
- Ajenifuja E, Ajao JA, Ajayi EOB (2017) Adsorption isotherm studies of Cu (II) and Co (II) in high concentration aqueous solutions on photocatalytically modified diatomaceous ceramic adsorbents. *Appl Water Sci* 7:3793–3801. <https://doi.org/10.1007/s13201>
- Awwad A M, Salem N M (2014) Kinetics and thermodynamics of Cd(II) biosorption onto loquat (*Eriobotrya japonica*) leaves. *J Saudi Chem Soc* 18 (5): 486–493. <https://doi.org/10.1016/j.jscs.2011.10.007>.
- Bhaumik R, Mondal NK (2016) Optimizing adsorption of fluoride from water by modified banana peel dust using response surface modelling approach. *Appl Water Sci* 6:115–135. <https://doi.org/10.1007/s13201-014-0211-9>
- Farhan SN, Khadom AA (2015) Biosorption of heavy metals from aqueous solutions by *Saccharomyces Cerevisiae*. *Int J Ind Chem* 6(2):119–130. <https://doi.org/10.1007/s40090-015-0038-8>
- Wei W, Wang Q, Li A, Yang J, Ma F, Pi S, Wu D (2016) Biosorption of Pb (II) from aqueous solution by extracellular polymeric substances extracted from *Klebsiella* sp. J1: adsorption behavior and mechanism assessment. *Sci Rep* 6:31575. <https://doi.org/10.1038/srep31575>

29. Zulkali MMD, Ahmad AI, Norulakmal NH, Sharifah NS (2006) Comparative studies of *Oryza sativa* L. husk and chitosan as lead adsorbent. *J Chem Technol Biotechnol* 81:1324–1327. <https://doi.org/10.1002/jctb.1429>
30. Sari A, Tuzen M, Uluözlü ÖD, Soylak M (2007) Biosorption of Pb(II) and Ni(II) from aqueous solution by lichen (*Cladonia furcata*) biomass. *Biochem Eng J* 37(2):151–158. <https://doi.org/10.1016/j.bej.2007.04.007>
31. Ronda A, Martín-Lara MA, Dionisio E, Blázquez G, Calero M (2013) Effect of lead in biosorption of copper by almond shell. *J Taiwan Inst Chem Eng* 44(3):466–473. <https://doi.org/10.1016/j.jtice.2012.12.019>
32. Mahamadi C, Nharingo T (2010) Competitive adsorption of Pb²⁺, Cd²⁺ and Zn²⁺ ions onto *Eichhornia crassipes* in binary and ternary systems. *Bioresour Technol* 101(3):859–864. <https://doi.org/10.1016/j.biortech.2009.08.097>
33. Gundogdu A, Ozdes D, Duran C, Bulut VN, Soylak M, Senturk HB (2009) Biosorption of Pb(II) ions from aqueous solution by pine bark (*Pinus brutia* Ten.). *Chem Eng Sci* 153(1-3):62–69. <https://doi.org/10.1016/j.ces.2009.06.017>
34. Naiya TK, Bhattacharya AK, Das SK (2008) Adsorption of Pb(II) by sawdust and neem bark from aqueous solutions. *Environ Prog* 27(3):313–328. <https://doi.org/10.1002/ep.10280>
35. Pavan FA, Mazzocato AC, Jacques RA, Dias SLP (2008) Ponkan peel: a potential biosorbent for removal of Pb(II) ions from aqueous solution. *Biochem. Eng. J* 40(2): 357–362. <https://doi.org/10.1016/j.bej.2008.01.004>

Publisher's Note Springer Nature remains neutral with regard to jurisdictional claims in published maps and institutional affiliations.